Journal of Artificial Intelligence and Control Systems CoSci Press

Article

Immersion and Invariance Adaptive Fault-Tolerant Attitude Control for a Coaxial Tilt-Rotor eVTOL Aircraft

Zheng Hou [1], Zongyang Lv [2,*], Yuhu Wu [1]

1 School of Control Science and Engineering, Dalian University of Technology, Dalian 116024, China

2 Department of Electrical and Computer Engineering, University of Alberta, Edmonton, AB T6G 1H9, Canada

Article History:

Received: 18 September 2025

Revised: 13 January 2026

Accepted: 28 January 2026

Published: 16 March 2026

Abstract: This paper proposes an adaptive fault-tolerant attitude control strategy based on the Immersion and Invariance (I&I) methodology for a Coaxial Tilt-Rotor (CTR) eVTOL aircraft. The CTR-eVTOL, equipped with two pairs of CTR modules and a rear rotor, exhibiting strong nonlinearity, underactuated, and strong coupling characteristics, faces significant challenges in maintaining stable attitude control when subjected to a Loss Of Effectiveness (LOE) fault. To address this, the proposed Fault-Tolerant Control (FTC) strategy integrates the I&I adaptive methodology to compensate for the torque losses induced by the LOE fault. Specifically, an I&I-based adaptive update law is designed to estimate the unknown faulty coefficient. The closed-loop system's asymptotic stability is theoretically proven using the Lyapunov method and LaSalle's invariance theorem. Real ground bench experiments with comparative controllers validate the effectiveness and superiority of the proposed FTC strategy.

Keywords: fault-tolerant control; tilt-rotor eVTOL; immersion and invariance

1. Introduction

In recent decades, electric Vertical TakeOff and Landing aircraft (eVTOL) have found extensive applications across diverse domains, such as payload transportation, surveillance, and military operations [1–3]. Among various eVTOL configurations, the Tilt-Rotor (TR) eVTOL has garnered significant attention due to its merits of faster response, higher agility, and greater flight speed [4,5]. Specifically, the Coaxial Tilt-Rotor (CTR) eVTOL, as illustrated in Figure 1, was introduced in [6], featuring two sets of coaxial rotor modules and a rear rotor. This special design provides advantages over single-rotor structures [7,8], including higher cruising speeds and a more compact structure. In addition, this configuration strengthens the control redundancy of the CTR-eVTOL, guaranteeing the controllability of the aircraft even in the event of rotor's total failure. In practical application, actuator faults are unavoidable in CTR-eVTOL operations, potentially causing degraded tracking performance or even severe accidents [9]. As a result, developing a robust fault-tolerant control scheme is imperative for boosting the CTR-eVTOL's safety.

In recent years, numerous research has been conducted on Fault-Tolerant Control (FTC) approaches. For example, Xian et al. [10] focused on a servo stuck fault scenario in a tilt-rotor Unmanned Aerial Vehicle (UAV), designing an observer to precisely estimate the specific parameters related to the stuck fault and offering a novel perspective on fault handling for this type of aircraft. Guo et al. [11] proposed an observer-based PD position controller and an observer-based sliding mode control attitude controller to achieve trajectory tracking for a UAV suffering with propeller damage. Nan et al. [12] designed a nonlinear model predictive controller to stabilize and control quadrotors during complete single-rotor failure.

Adaptive control technology has been applied to address the actuator faults in aircraft. Chen et al. [13] proposed a robust nonlinear controller which combines the sliding-mode

* Corresponding author: Zongyang Lv, Department of Electrical and Computer Engineering, University of Alberta, Edmonton, AB T6G 1H9, Canada, zongyan3@ualberta.ca

control technique to address the rotor faults. Wang et al. [14] regarded rotor faults as lumped external disturbances and developed an ASMC, effectively addressing rotor faults in multi-rotor aircraft. However, the classical adaptive controllers always require the Linear Parameterization condition and will lead to the singularity problem in the controller [15]. To overcome the aforementioned issues, an Immersion and Invariance (I&I)-based adaptive control strategy was first researched in [16]. The I&I adaptive controller can simplify the stability analysis by introducing cross terms in the Lyapunov function [17]. Furthermore, it introduces a cross term between the parameter estimates and the plant states, which enhances the convergence performance of the parameter estimation. The I&I adaptive controller has then been further developed by many researchers and applied in various fields, such as aircraft control. In [18], an I&I-based adaptive control methodology is designed to compensate for the parametric uncertainties of a quadrotor to realize the position tracking. An I&I-based adaptive attitude controller is proposed for the tilt-rotor aircraft, where an adaptive update law is specially designed to compensate for the uncertainties of damping coefficients [19].

Inspired by the I&I technique [16,17], an I&I-based Attitude Fault-Tolerant Control (IIAFTC) strategy for the specific CTR-eVTOL configuration is proposed, enabling precise attitude tracking under a Loss of Effectiveness (LOE) fault. The contributions of this paper are twofold:

(1) In contrast to existing works [11,13,14] that only estimate or compensate for lumped disturbances induced by rotor faults, the proposed IIAFTC strategy achieves accurate estimation of the actual LOE faulty coefficient of the faulty rotor. This coefficient directly characterizes the rotor's degradation degree, which is critical for three key aspects: 1) enhancing attitude control precision by quantifying fault impacts; 2) accelerating transient response via targeted compensation; 3) supporting post-fault logical decision-making. Leveraging this estimation, the proposed strategy precisely calculates and compensates for the fault's impact on the attitude control system, thereby achieving attitude control under LOE faults.

(2) Ground bench experiments are conducted to validate the effectiveness of the proposed strategy, covering 30%, 70%, and 100% LOE fault severities. Comparative tests against the traditional adaptive controller and adaptive sliding mode controller further demonstrate its superiority.

2. Model of the CTR-eVTOL Under a Rotor's LOE Fault

This paper presents two coordinate systems, specifically the body-fixed frame B and the inertial frame E, as depicted in Figure 1.

The Euler angles are denoted by $\boldsymbol{\eta}=[\phi,\theta,\psi]^\top$, where ϕ, θ, and ψ represent the roll, pitch, and yaw angles of the CTR-eVTOL, respectively. The vector $\boldsymbol{v}=[v_x,v_y,v_z]^\top$ denotes the velocity of the CTR-eVTOL's center of gravity (CoG) in the inertial frame E.Throughout this study, $\boldsymbol{s}*$, $\boldsymbol{c}*$, and $\boldsymbol{t}*$ denote $\sin(*)$, $\cos(*)$, and $\tan(*)$, respectively. The symbol $\boldsymbol{0}_{m\times n}$ represents an $m\times n$ zero matrix, while $\boldsymbol{I}_n$ signifies an n-dimensional identity matrix. For a matrix $\boldsymbol{A}\in\mathbb{R}^{m\times n}$, $\boldsymbol{A}^\top$ denotes its transpose, and $\lambda_{\mathrm{m}}(\boldsymbol{A})$ represents the smallest eigenvalue of $\boldsymbol{A}$.

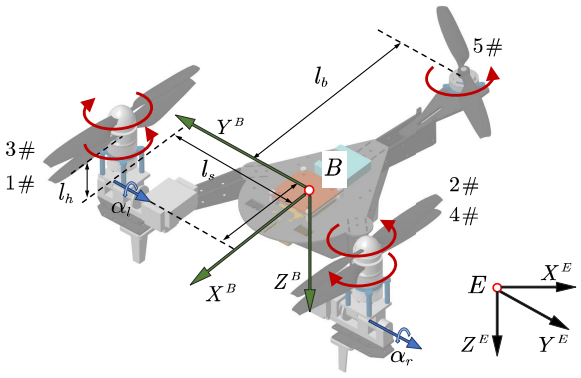

Figure 1. The schematic of the CTR-eVTOL with reference frames.

2.1. Attitude Model of the CTR-eVTOL

The Euler angular velocity is obtained as:

$$\dot{\boldsymbol{\eta}}=\left[\dot{\phi},\dot{\theta},\dot{\psi}\right]^\top=\boldsymbol{T}_r^{-1}\boldsymbol{\omega},$$

where $\boldsymbol{\omega}=[p,q,r]^\top$ denotes the angular velocity in the body-fixed frame. The transformation matrix $\boldsymbol{T}_r$ is represented as [20]

$$\boldsymbol{T}_r=\begin{bmatrix}1 & 0 & -\boldsymbol{s}\theta\\ 0 & \boldsymbol{c}\phi & \boldsymbol{s}\phi\boldsymbol{c}\theta\\ 0 & -\boldsymbol{s}\phi & \boldsymbol{c}\phi\boldsymbol{c}\theta\end{bmatrix}. \tag{1}$$

Based on Newton's second law, the rotational dynamic model of the CTR-eVTOL without rotor fault is written as

$$\ddot{\boldsymbol{\eta}}=\boldsymbol{T}_r^{-1}\boldsymbol{J}^{-1}(\boldsymbol{\omega}\times\boldsymbol{J}\boldsymbol{\omega}+\boldsymbol{\tau}+\boldsymbol{\tau}_\alpha+\boldsymbol{D}_\eta)-\boldsymbol{T}_r^{-1}\dot{\boldsymbol{T}}_r\dot{\boldsymbol{\eta}}, \tag{2}$$

where the term $\boldsymbol{\tau}$ is the control torque and the term $\boldsymbol{D}_\eta$ denotes the drag torque. The torque generated by the servos is

given as $\boldsymbol{\tau_\alpha} = [0, \tau_r + \tau_l, 0]^\top$, where τ_r and τ_l are the rotational torques caused by the right and left servos, respectively. The inertia matrix $\boldsymbol{J} = \boldsymbol{T_r}^\top \boldsymbol{I} \boldsymbol{T_r}$, with $\boldsymbol{I} = \begin{bmatrix} I_x & 0 & -I_{xz} \\ 0 & I_y & 0 \\ -I_{xz} & 0 & I_z \end{bmatrix}$.

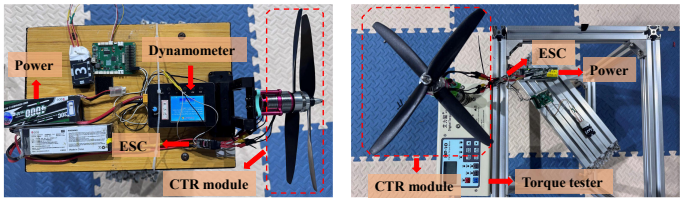

(a) Self-built platform for thrust and torque measurements.

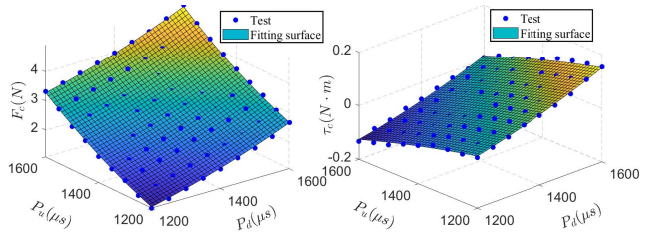

(b) Fitting results of the thrust and torque.

Figure 2. Measurements and fitting results of the CTR module.

The thrust and torque of rear rotor $5\#$ are related to its PWM signal $P_i(1050\mu s \sim 1950\mu s)$ as:

$$F_5 = c_{f5}(P_5 - 1050)^2, \quad \tau_5 = c_{t5}(P_i - 1050)^2, \tag{3}$$

where c_{f5} and c_{t5} are the thrust and torque coefficients of the rotor $5\#$, respectively.

Considering the coupling effect between the upper rotor and the lower rotor due to the downwash effect in a CTR module, the thrust and torque coefficients of the upper rotor are different from those of the lower rotor. Then, we measured the thrust and torque of the CTR module under varying PWM signals using our self-built platform, as shown in Figure 2(a). Based on the measured data, the quadratic surfaces are constructed to fit these data in order to establish a precise CTR thrust and torque model that accounts for the coupling between upper and lower rotors. Subsequently, the thrust $F_c, c = l, r$ and torque $\tau_c, c = l, r$ of a single CTR module are modeled as

$$\begin{aligned} F_c(P_u, P_d) &= \underbrace{c_{fu}(P_u - 1050)^2}_{F_u} + \underbrace{c_{fd}(P_d - 1050)^2}_{F_d}, \\ \tau_c(P_u, P_d) &= \underbrace{c_{tu}(P_u - 1050)^2}_{\tau_u} - \underbrace{c_{td}(P_d - 1050)^2}_{\tau_d}, \end{aligned} \tag{4}$$

where the terms P_u and P_d represent the PWM signals of the upper rotor and the lower rotor in one CTR module, respectively; the parameters c_{fu} and c_{tu} are the thrust and torque coefficients of the upper rotor, while the parameters c_{fd} and c_{td} are the thrust and torque coefficients of the lower rotor. By using least squares method, the coefficients are determined as $c_{fu} = 0.8402 \times 10^{-5}$, $c_{fd} = 1.059 \times 10^{-5}$, $c_{tu} = 1.024 \times 10^{-7}$, and $c_{td} = 0.9325 \times 10^{-7}$, as shown in Figure 2(b).

The force $\boldsymbol{F_{xzb}} = [F_{xb}, F_{zb}]^\top$ represents the thrust produced by the rotors in the body-fixed frame. The force $\boldsymbol{F_{xzb}}$ and control torque $\boldsymbol{\tau}$ in (2) of the CTR-eVTOL are derived as

$$\begin{bmatrix} F_{xb} \\ F_{zb} \\ \tau_\phi \\ \tau_\theta \\ \tau_\psi \end{bmatrix} = \begin{bmatrix} F_r \boldsymbol{s}\alpha_r + F_l \boldsymbol{s}\alpha_l \\ -F_r \boldsymbol{c}\alpha_r - F_l \boldsymbol{c}\alpha_l - F_5 \\ -F_r \boldsymbol{c}\alpha_r l_s + F_l \boldsymbol{c}\alpha_l l_s - \tau_r \boldsymbol{s}\alpha_r - \tau_l \boldsymbol{s}\alpha_l \\ F_r \boldsymbol{c}\alpha_r l_f + F_l \boldsymbol{c}\alpha_l l_f - F_5 l_b - F_r \boldsymbol{s}\alpha_r l_h - F_l \boldsymbol{s}\alpha_l l_h \\ -F_r \boldsymbol{s}\alpha_r l_s + F_l \boldsymbol{s}\alpha_l l_s + \tau_5 + \tau_r \boldsymbol{c}\alpha_r + \tau_l \boldsymbol{c}\alpha_l \end{bmatrix}, \tag{5}$$

where the terms F_r, F_l, τ_r, and τ_l represent the command thrust of the right CTR module, the command thrust of the left CTR module, the command torque of the right CTR module, and the command torque of the left CTR module, respectively; the terms l_s, l_f, l_b, and l_h are the geometric parameters of the CTR-eVTOL shown in Figure 1; α_r and α_l are the tilt angles of the right and left CTR modules. Furthermore, F_r, τ_r, F_l, and τ_l are expressed as $F_r = F_1 + F_3$, $\tau_r = \tau_3 - \tau_1$, $F_l = F_2 + F_4$, and $\tau_l = \tau_4 - \tau_2$.

2.2. Model of the CTR-eVTOL Under an LOE Fault

As one of the most common types of faults in aircraft systems [21], a rotor's LOE fault is considered in this paper. For instance, aging and abrasion of the rotor will cause unexpected changes in its thrust and torque performance, ultimately resulting in LOE faults. The fault model of an LOE fault in the rotor $i\#$ is designed as

$$F_i^* = (1 - \Gamma_i) F_i, \quad \tau_i^* = (1 - \Gamma_i) \tau_i, \tag{6}$$

where the terms F_i and $\tau_i (i = 1, 2, 3, 4)$ represent the command thrust and torque of the rotor i generated by the control allocation; the terms F_i^* and τ_i^* are the actual thrust and torque under an LOE fault in the rotor i, and the unknown parameter $\Gamma_i \in [0, 1]$ $(i = 1, 2, 3, 4)$ represents the faulty coefficient of the rotor $i\#$. For instance, the case

$\Gamma_i = 0$ indicates that the rotor is healthy, and the case $\Gamma_i = 1$ indicates that the rotor is completely damaged. It is worth noting that the faulty coefficient Γ_i is unknown.

Then, by replacing F_i and τ_i in the force/torque model (5) with F_i^* and τ_i^*, the model of the CTR-eVTOL under an LOE fault of the rotor $i\#$ is derived. Extracting the control torque from model (5), the following expression is obtained:

$$\begin{bmatrix} \tau_\phi \\ \tau_\theta \\ \tau_\psi \end{bmatrix} = \begin{bmatrix} -F_r \boldsymbol{c}\alpha_r l_s + F_l \boldsymbol{c}\alpha_l l_s - \tau_r \boldsymbol{s}\alpha_r - \tau_l \boldsymbol{s}\alpha_l \\ F_r \boldsymbol{c}\alpha_r l_f + F_l \boldsymbol{c}\alpha_l l_f - F_5 l_b - F_r \boldsymbol{s}\alpha_r l_h - F_l \boldsymbol{s}\alpha_l l_h \\ -F_r \boldsymbol{s}\alpha_r l_s + F_l \boldsymbol{s}\alpha_l l_s + \tau_5 + \tau_r \boldsymbol{c}\alpha_r + \tau_l \boldsymbol{c}\alpha_l \end{bmatrix} - \Gamma_i \boldsymbol{\delta_i}, \tag{7}$$

where the tilt angles α_i are defined as $\alpha_1 = \alpha_4 = \alpha_r$ and $\alpha_2 = \alpha_3 = \alpha_l$; the matrices $\boldsymbol{\delta_i}$ are defined as

$$\boldsymbol{\delta_i} = F_i \begin{bmatrix} (-1)^{i^*+1} c_{tfi} \boldsymbol{s}\alpha_i + (-1)^i l_s \boldsymbol{c}\alpha_i \\ -l_h \boldsymbol{s}\alpha_i + l_f \boldsymbol{c}\alpha_i \\ (-1)^i l_s \boldsymbol{s}\alpha_i + (-1)^{i^*} c_{tfi} \boldsymbol{c}\alpha_i \end{bmatrix},$$

where the term $i^* = \mathrm{quot}(i, 2) + 1$, and the coefficients c_{tfi} are expressed as $c_{tf1} = c_{tf3} = c_{td}/c_{fd}$ and $c_{tf2} = c_{tf4} = c_{tu}/c_{fu}$. The term F_i represents the control thrust of the rotor $i\#$ generated by the control allocation method.

Then, substituting the LOE fault torque model (7) into the attitude dynamic model (2), the following fault model of the CTR-eVTOL under an LOE fault in the rotor $i\#$ is derived as

$$\ddot{\boldsymbol{\eta}} = \boldsymbol{f_\eta} + \boldsymbol{g_\eta}(\boldsymbol{\tau} - \Gamma_i \boldsymbol{\delta_i}), \tag{8}$$

where the nonlinear functions

$$\begin{aligned} \boldsymbol{f_\eta} &= \boldsymbol{T_r^{-1}} \boldsymbol{J^{-1}} (\boldsymbol{\omega} \times \boldsymbol{J\omega} + \boldsymbol{\tau_\alpha} + \boldsymbol{D_\eta}) - \boldsymbol{T_r^{-1}} \dot{\boldsymbol{T}}_r \dot{\boldsymbol{\eta}}, \\ \boldsymbol{g_\eta} &= \boldsymbol{T_r^{-1}} \boldsymbol{J^{-1}}, \end{aligned} \tag{9}$$

with the term $\Gamma_i F_i \boldsymbol{\delta_{\eta i}}$ representing the impact caused by the LOE fault.

Assumption 1. *The faulty coefficient Γ_i is considered as a constant after LOE fault occurrence [17], and this constant is unknown.*

Remark 1. *It is reasonable to assume the faulty coefficient as an unknown constant for certain degradation scenarios such as rotor aging and abrasion [17]. For multi-stage LOE fault scenarios with a piecewise-constant faulty coefficient, the proposed IIAFTC strategy theoretically enables re-estimation of the faulty coefficient Γ_i at each new stage, thus maintaining applicability.*

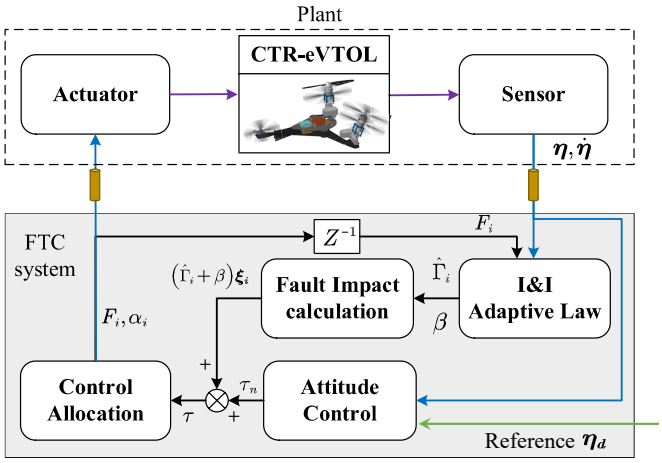

Figure 3. The schematic of the IIAFTC strategy.

3. IIAFTC Strategy Design

The control objective of this paper is as follows: For a CTR-eVTOL with strong nonlinearity, underactuated nature, and strong coupling characteristics, under an LOE fault with an unknown faulty coefficient Γ_i, design an adaptive control input $\boldsymbol{\tau}$ in Eq. (8) to ensure that the actual attitude $\boldsymbol{\eta}$ tracks the desired attitude $\boldsymbol{\eta_d}$ and accurately estimates the faulty coefficient Γ_i.

Then, the IIAFTC strategy is designed based on the attitude dynamic model (8) in the presence of an LOE fault in the rotor $i\#$ with unknown faulty coefficient Γ_i. By applying the proposed IIAFTC strategy, the unknown faulty coefficient Γ_i can be accurately estimated when system meets the persistent-excitation condition [15], and the desired attitude $\boldsymbol{\eta_d}$ can be accurately tracked under an LOE fault. And the control allocation is designed which considers the coupling effect in CTR module.

3.1. Control Allocation

Considering this characteristic and the distinct dynamic behaviors of the rotors and servos, two constraints are designed as $\alpha_r = \alpha_l = \alpha$ and $F_1 + F_4 = F_2 + F_3$. Then, the control allocation law is solved as

$$\begin{aligned} F_5 &= \frac{F_{zb} l_f + F_{xb} l_h + \tau_\theta}{-l_f - l_b}, \alpha = \arctan\left(\frac{-F_{xb}}{F_{zb} + F_5}\right), \\ F_1 &= ((c_{tfd} + c_{tfu}) l_s A - 2c_{tfu} \boldsymbol{s}\alpha B - 2\tau_\phi \boldsymbol{c}\alpha c_{tfu} \\ &\quad -2l_s \boldsymbol{c}\alpha B + 2l_s \tau_\phi \boldsymbol{s}\alpha)/(4l_s(c_{tfd} + c_{tfu})), \\ F_2 &= ((c_{tfd} + c_{tfu}) l_s A + 2c_{tfd} \boldsymbol{s}\alpha B + 2\tau_\phi \boldsymbol{c}\alpha c_{tfd} \\ &\quad -2l_s \boldsymbol{c}\alpha B + 2l_s \tau_\phi \boldsymbol{s}\alpha)/(4l_s(c_{tfd} + c_{tfu})), \\ F_3 &= ((c_{tfd} + c_{tfu}) l_s A - 2c_{tfd} \boldsymbol{s}\alpha B - 2\tau_\phi \boldsymbol{c}\alpha c_{tfd} \\ &\quad +2l_s \boldsymbol{c}\alpha B - 2l_s \tau_\phi \boldsymbol{s}\alpha)/(4l_s(c_{tfd} + c_{tfu})), \\ F_4 &= ((c_{tfd} + c_{tfu}) l_s A + 2c_{tfu} \boldsymbol{s}\alpha B + 2\tau_\phi \boldsymbol{c}\alpha c_{tfu} \\ &\quad +2l_s \boldsymbol{c}\alpha B - 2l_s \tau_\phi \boldsymbol{s}\alpha)/(4l_s(c_{tfd} + c_{tfu})), \end{aligned} \tag{10}$$

where the terms A and B satisfy $A=(\tau_\theta+F_5 l_b)/(l_f \boldsymbol{c}\alpha - l_h \boldsymbol{s}\alpha)$ and $B=\tau_\psi - c_{t5}F_5/c_{f5}$; the coefficients $c_{tfu}= c_{tu}/c_{fu}$ and $c_{tfd}=c_{td}/c_{fd}$. According to the above control allocation, the tilt angle α is exclusively utilized for adjusting the component forces F_{xb} and F_{zb}. Hence, the proposed control allocation diminishes vibrations arising from adjusting the tilt angles α_r and α_l, and extends the mechanical lifespan of the servos.

Remark 2. *In addition, the designed two constraints have considered the energy consumption problem. Under the designed two constraints, the inefficient internal force cancellation problem is avoided by not performing differential tilting (i.e., $\alpha_r \neq \alpha_l$), as described in [7]. Therefore, the analytical control allocation by adding the designed two constraints optimizes the energy consumption to a certain extent.*

3.2. Adaptive Attitude Controller

To achieve attitude tracking under an LOE fault, an adaptive attitude controller is designed based I&I methodology. Let $\boldsymbol{\eta_d}$ denote the desired attitude angle, which has a second-order continuous derivative. The associated tracking errors $\boldsymbol{e_\eta}$ and $\boldsymbol{e_{d\eta}}$ are defined as follows:

$$\boldsymbol{e_\eta}=\boldsymbol{\eta}-\boldsymbol{\eta_d}, \tag{11a}$$

$$\boldsymbol{e_{d\eta}}=\dot{\boldsymbol{e}}_\eta+\boldsymbol{\alpha_\eta e_\eta}, \tag{11b}$$

where $\boldsymbol{\alpha_\eta}=\mathrm{diag}(\alpha_\phi,\alpha_\theta,\alpha_\psi)$ is a positive definite diagonal matrix. Substituting the attitude dynamic model (8) into the time derivative of (11b) yields

$$\dot{\boldsymbol{e}}_\eta=\boldsymbol{e_{d\eta}}-\boldsymbol{\alpha_\eta e_\eta}. \tag{12a}$$

$$\dot{\boldsymbol{e}}_{d\eta}=\boldsymbol{f_\eta}+\boldsymbol{g_\eta}(\boldsymbol{\tau}-\Gamma_i F_i \boldsymbol{\delta_{\eta i}} \boldsymbol{k_{\alpha i}})-\ddot{\boldsymbol{\eta}}_d+\boldsymbol{\alpha_\eta}\dot{\boldsymbol{e}}_\eta. \tag{12b}$$

Define the estimation error $\tilde{\Gamma}_i$ as

$$\tilde{\Gamma}_i=\hat{\Gamma}_i-\Gamma_i+\beta(\boldsymbol{e_\eta},\boldsymbol{e_{d\eta}}), \tag{13}$$

where $\hat{\Gamma}_i$ is the estimate of the faulty coefficient Γ_i, and β is an auxiliary function. After differentiating (13) with respect to time, we have

$$\dot{\tilde{\Gamma}}_i=\dot{\hat{\Gamma}}_i-\dot{\Gamma}_i+\frac{\partial\beta}{\partial \boldsymbol{e_\eta}}\dot{\boldsymbol{e}}_\eta+\frac{\partial\beta}{\partial \boldsymbol{e_{d\eta}}}\dot{\boldsymbol{e}}_{d\eta}. \tag{14}$$

Then, substituting dynamic model of the error system (12a) and (12b) into the above equation, the following expression is obtained:

$$\begin{aligned}\dot{\tilde{\Gamma}}_i=&\dot{\hat{\Gamma}}_i-\dot{\Gamma}_i+\frac{\partial\beta}{\partial \boldsymbol{e_\eta}}\dot{\boldsymbol{e}}_\eta\\&+\frac{\partial\beta}{\partial \boldsymbol{e_{d\eta}}}(\boldsymbol{f_\eta}+\boldsymbol{g_\eta}\boldsymbol{\tau}-\Gamma_i\boldsymbol{g_\eta}\boldsymbol{\xi_i}-\ddot{\boldsymbol{\eta}}_d+\boldsymbol{\alpha_\eta}\dot{\boldsymbol{e}}_\eta),\end{aligned} \tag{15}$$

where the term $\boldsymbol{\xi_i}=F_i\boldsymbol{\delta_{\eta i}}\boldsymbol{k_{\alpha i}}$. It is desired for the estimation error to asymptotically converge to zero, thus the adaptive update law is designed as

$$\begin{aligned}\dot{\hat{\Gamma}}_i=&-\frac{\partial\beta}{\partial \boldsymbol{e_\eta}}\dot{\boldsymbol{e}}_\eta-\frac{\partial\beta}{\partial \boldsymbol{e_{d\eta}}}(\boldsymbol{f_\eta}+\boldsymbol{g_\eta}\boldsymbol{\tau}-\ddot{\boldsymbol{\eta}}_d+\boldsymbol{\alpha_\eta}\dot{\boldsymbol{e}}_\eta)\\&+\frac{\partial\beta}{\partial \boldsymbol{e_{d\eta}}}\left(\hat{\Gamma}_i+\beta\right)\boldsymbol{g_\eta}\boldsymbol{\xi_i}.\end{aligned} \tag{16}$$

Then, substituting the adaptive update law (16) into the dynamics (15) of the estimation error yields

$$\dot{\tilde{\Gamma}}_i=\frac{\partial\beta}{\partial \boldsymbol{e_{d\eta}}}\boldsymbol{g_\eta}\boldsymbol{\xi_i}\tilde{\Gamma}_i-\dot{\Gamma}_i. \tag{17}$$

Then, to realize the convergence of the estimation error $\tilde{\Gamma}_i$, the auxiliary function is designed as

$$\beta=-K_o(\boldsymbol{\xi_i}\boldsymbol{g_\eta})^\top \boldsymbol{e_{d\eta}}, \tag{18}$$

where K_o is a positive scalar. The control torque $\boldsymbol{\tau}$ is designed in the following two parts

$$\boldsymbol{\tau}=\boldsymbol{\tau_n}+\left(\hat{\Gamma}_i+\beta\right)\boldsymbol{\xi_i}, \tag{19}$$

where

$$\boldsymbol{\tau_n}=\boldsymbol{g_\eta}^{-1}\left(-(\boldsymbol{k_{\eta 1}}+\boldsymbol{\alpha_\eta})\boldsymbol{e_\eta}-\boldsymbol{k_{\eta 2}}\boldsymbol{e_{d\eta}}-\boldsymbol{f_\eta}+\ddot{\boldsymbol{\eta}}_d\right), \tag{20}$$

with $\boldsymbol{k_{\eta 1}}=\mathrm{diag}(k_{\phi 1},k_{\theta 1},k_{\psi 1})$ and $\boldsymbol{k_{\eta 2}}=\mathrm{diag}(k_{\phi 2},k_{\theta 2},k_{\psi 2})$ are positive-definite diagonal matrices. In (19), the term $\left(\hat{\Gamma}_i+\beta\right)\boldsymbol{\xi_i}$ is calculated by the fault impact calculation module to compensate for the LOE fault. Compared to [13], [14], [22], and [23], the proposed strategy extracts and estimates the faulty coefficient Γ_i from the lumped disturbances $\left(\hat{\Gamma}_i+\beta\right)\boldsymbol{\xi_i}$ caused by an LOE fault, **achieving** quantitative evaluation of the severity of rotor faults rather than **estimating** the lumped disturbances.

Theorem 1. *Considering the CTR-eVTOL's attitude dynamic (8) under an LOE fault in rotor $i\#$, and utilizing the control torque (19) and adaptive law (16), then the tracking errors and are asymptotically stable in the sense that*

$$\boldsymbol{e_\eta}\to\boldsymbol{0},\ \boldsymbol{e_{d\eta}}\to\boldsymbol{0}\ \ as\ \ t\to\infty. \tag{21}$$

Proof of Theorem 1. Based on Assumption 1 and substituting (18) into (17), the following dynamics of the estimation error

$\tilde{\Gamma}_i$ is obtained as

$$\dot{\tilde{\Gamma}}_i = -K_o(\boldsymbol{g_\eta \xi_i})^\top \boldsymbol{g_\eta \xi_i}\tilde{\Gamma}_i. \tag{22}$$

By substituting control torque (20) into (12b), the dynamics of the tracking errors is formulated as

$$\dot{\boldsymbol{e}}_{d\eta} = -\boldsymbol{k}_{\eta 1}\boldsymbol{e}_\eta - \boldsymbol{k}_{\eta 2}\boldsymbol{e}_{d\eta} + \tilde{\Gamma}_i \boldsymbol{g_\eta \xi_i}, \tag{23}$$

In order to verify the convergence of parameter estimation error, let denote the following nonnegative function:

$$V_\Gamma = \frac{1}{2}\tilde{\Gamma}_i^2. \tag{24}$$

According to the definition of $\boldsymbol{g_\eta \xi_i} = [\epsilon_{\phi i}, \epsilon_{\theta i}, \epsilon_{\psi i}]^\top \in \mathbb{R}^{3\times 1}$, and substituting the dynamic (22) into the time derivative of function (24), the following expression is obtained as

$$\begin{aligned}\dot{V}_\Gamma &= -K_o(\boldsymbol{g_\eta \xi_i})^\top \boldsymbol{g_\eta \xi_i}\tilde{\Gamma}_i^2 \\ &= -K_o(\epsilon_{\phi i}^2 + \epsilon_{\theta i}^2 + \epsilon_{\psi i}^2)\tilde{\Gamma}_i^2 \le 0.\end{aligned} \tag{25}$$

It is concluded that $\tilde{\Gamma}_i \boldsymbol{g_\eta \xi_i} \in \mathbf{L}_2$. Then, it is obvious that the estimation error $\tilde{\Gamma}_i$ is bounded. To verify the convergence property of the whole closed-loop system, define a Lyapunov function candidate as follows:

$$V_\eta = \frac{1}{2}\boldsymbol{e}_\eta^\top \boldsymbol{k}_{\eta 1}\boldsymbol{e}_\eta + \frac{1}{2}\boldsymbol{e}_{d\eta}^\top \boldsymbol{e}_{d\eta} + \frac{1}{2}k_2^{-1}K_o^{-1}\tilde{\Gamma}_i^2, \tag{26}$$

where $k_2 = \lambda_{\min}(\boldsymbol{k}_{\eta 2})$. Taking the time derivative of (26), we have

$$\begin{aligned}\dot{V}_\eta &= -\boldsymbol{e}_\eta^\top \boldsymbol{k}_{\eta 1}\dot{\boldsymbol{e}}_\eta + \boldsymbol{e}_{d\eta}^\top \dot{\boldsymbol{e}}_{d\eta} + k_2^{-1}K_o^{-1}\tilde{\Gamma}_i\dot{\tilde{\Gamma}}_i \\ &= -\boldsymbol{e}_\eta^\top \boldsymbol{\alpha}_\eta \boldsymbol{e}_\eta - \boldsymbol{e}_{d\eta}^\top \boldsymbol{k}_{\eta 2}\boldsymbol{e}_{d\eta} + \boldsymbol{e}_{d\eta}^\top \tilde{\Gamma}_i \boldsymbol{g_\eta \xi_i} \\ &\quad -k_2^{-1}(\boldsymbol{g_\eta \xi_i})^\top \boldsymbol{g_\eta \xi_i}\tilde{\Gamma}_i^2 \\ &\le -\boldsymbol{e}_\eta^\top \boldsymbol{\alpha}_\eta \boldsymbol{e}_\eta - k_2 \boldsymbol{e}_{d\eta}^\top \boldsymbol{e}_{d\eta} + \boldsymbol{e}_{d\eta}^\top \tilde{\Gamma}_i \boldsymbol{g_\eta \xi_i} \\ &\quad -k_2^{-1}(\boldsymbol{g_\eta \xi_i})^\top \boldsymbol{g_\eta \xi_i}\tilde{\Gamma}_i^2 \\ &\le -\boldsymbol{e}_\eta^\top \boldsymbol{\alpha}_\eta \boldsymbol{e}_\eta - \frac{1}{2}k_2 \boldsymbol{e}_{d\eta}^\top \boldsymbol{e}_{d\eta} - \frac{1}{2}k_2^{-1}(\boldsymbol{g_\eta \xi_i})^\top \boldsymbol{g_\eta \xi_i}\tilde{\Gamma}_i^2 \\ &\quad -\frac{1}{2}\left(k_2 \boldsymbol{e}_{d\eta}^\top \boldsymbol{e}_{d\eta} - 2\boldsymbol{e}_{d\eta}^\top \tilde{\Gamma}_i \boldsymbol{g_\eta \xi_i} + k_2^{-1}(\boldsymbol{g_\eta \xi_i})^\top \boldsymbol{g_\eta \xi_i}\tilde{\Gamma}_i^2\right) \\ &\le -\boldsymbol{e}_\eta^\top \boldsymbol{\alpha}_\eta \boldsymbol{e}_\eta - \frac{1}{2}k_2 \boldsymbol{e}_{d\eta}^\top \boldsymbol{e}_{d\eta} - \frac{1}{2}k_2^{-1}(\boldsymbol{g_\eta \xi_i})^\top \boldsymbol{g_\eta \xi_i}\tilde{\Gamma}_i^2 \\ &\quad -\frac{1}{2}\left(k_2^{\frac{1}{2}}\boldsymbol{e}_{d\eta} - k_2^{-\frac{1}{2}}\boldsymbol{g_\eta \xi_i}\tilde{\Gamma}_i\right)^\top \left(k_2^{\frac{1}{2}}\boldsymbol{e}_{d\eta} - k_2^{-\frac{1}{2}}\boldsymbol{g_\eta \xi_i}\tilde{\Gamma}_i\right) \\ &\le -\boldsymbol{e}_\eta^\top \boldsymbol{\alpha}_\eta \boldsymbol{e}_\eta - \frac{1}{2}k_2 \boldsymbol{e}_{d\eta}^\top \boldsymbol{e}_{d\eta} - \frac{1}{2}k_2^{-1}(\boldsymbol{g_\eta \xi_i})^\top \boldsymbol{g_\eta \xi_i}\tilde{\Gamma}_i^2 \\ &\le 0\end{aligned} \tag{26}$$

Then, based on LaSalle's invariance theorem, all the trajectories of the close-loop system converge to the following invariant set:

$$M = \{(\boldsymbol{e}_\eta, \boldsymbol{e}_{d\eta}, \tilde{\Gamma}_i) : \boldsymbol{e}_\eta = \boldsymbol{0},\ \boldsymbol{e}_{d\eta} = \boldsymbol{0},\ \boldsymbol{g_\eta \xi_i}\tilde{\Gamma}_i = \boldsymbol{0}\}. \tag{27}$$

Hence, the closed-loop has a stable equilibrium at $[\boldsymbol{e}_\eta^\top, \boldsymbol{e}_{d\eta}^\top]^\top = [0_{3\times 1}, 0_{3\times 1}]^\top \in \mathbb{R}^6$. That means the result in (21) is proved.

Remark 3. *As shown in (16), compared with the traditional adaptive method, the dynamics of the estimation error designed by the I&I methodology is not only related to the state of the system, but also related to the estimation error itself. This characteristic enhances the robustness and transient response performance of the CTR-eVTOL system. The estimated faulty coefficient $\hat{\Gamma}_i + \beta$ is used to compensate for the LOE fault and theoretically guarantee the stability of the system. In fact, according to (22), the system satisfies the persistent-excitation condition [15], thus it is concluded that the estimated faulty coefficient $\hat{\Gamma}_i$ will converge to Γ_i.*

In summary, when an LOE fault occurs in one rotor, the proposed IIAFTC strategy enables compensation for the torque losses caused by the LOE fault based on the I&I adaptive law. A control allocation is developed according to the special configuration of the CTR-eVTOL. Collectively, these components constitute the IIAFTC strategy, and the corresponding algorithm is summarized as in Algorithm 1.

Algorithm 1. I&I-based Attitude Fault-Tolerant Control Strategy.

Algorithm 1 I&I-based Attitude Fault-Tolerant Control (IIAFTC)

Input: Predefined desired attitude $\boldsymbol{\eta_d}$, physical parameters of the CTR-eVTOL (e.g., m, l_s, l_f, l_b, and l_h), control gains ($\boldsymbol{k}_{\eta 1}$, $\boldsymbol{k}_{\eta 2}$, $\boldsymbol{\alpha}_\eta$, K_o).

Output: PWM signals for all actuators.

Initialization:

Set initial estimation of faulty coefficient $\hat{\Gamma}_i = 0$, stabilize the CTR-eVTOL on the ground bench.

1. At each sampling step, collect measured $\boldsymbol{\eta}$ and $\boldsymbol{\omega}$ from the IMU; compute $\dot{\boldsymbol{\eta}} = \boldsymbol{T_r}^{-1}\boldsymbol{\omega}$, via transformation matrix $\boldsymbol{T_r}$ (Eq. (1)).
2. Compute tracking errors $\boldsymbol{e}_\eta$ and $\boldsymbol{e}_{d\eta}$ from the Eq. (11a) and (11b).
3. Calculate auxiliary function β from Eq. (18).
4. Update $\hat{\Gamma}_i$ using the I&I adaptive law.
5. Compute the control torque $\boldsymbol{\tau}$ by using the updated

faulty coefficient $\hat{\Gamma}_i$.

6. Solve for rotor thrusts F_i and tilt angle α via Eq. (10).
7. Map rotor thrusts to PWM signals P_i using the established thrust model (Eqs. (3)-(4)).
8. Output PWM signals to rotors and servos, and return to Step 1 for the next sampling cycle.

4. Experimental Results

In this section, ground bench experiments are first implemented on a CTR-eVTOL to validate its attitude tracking performance under a rotor LOE fault, and a real-time flight experiment is then conducted in an indoor environment. The physical parameters of the actual CTR-eVTOL aircraft are listed as follows: $m=0.979kg$, $l_f=0.078m$, $l_b=0.24m$, $l_s=0.151m$, $l_h=0.0142m$, $I_x=4.11\cdot10^{-3}kg\cdot m^2$, $I_y=6.3\cdot10^{-3}kg\cdot m^2$, $I_z=9.85\cdot10^{-3}kg\cdot m^2$, and $I_{xz}=0.54\cdot10^{-3}kg\cdot m^2$.

Two comparative methods, involving an adaptive controller and an ASMC, are implemented in ground bench experiments to demonstrate the superiority of the proposed IIAFTC strategy. The control parameters for the adaptive control (AC), ASMC controller, and the control gains $\boldsymbol{k_{\eta 1}}$, $\boldsymbol{k_{\eta 2}}$, and $\boldsymbol{\alpha_\eta}$ are tuned using the Ziegler-Nichols Tuning Rules [24]. The objective function for control parameter tuning is the root mean square error (RMSE) of the tracking errors. Then, the parameter K_o is adjusted to ensure rapid convergence of the estimation error of the faulty coefficient Γ_i while limiting overshoot to within 5% and avoiding high-frequency oscillations. The detailed control parameters of the IIAFTC strategy are provided as: $\boldsymbol{k_{\eta 1}}=\mathrm{diag}(36,35,5)$, $\boldsymbol{k_{\eta 2}}=\mathrm{diag}(1.0,1.0,0.2)$, $\boldsymbol{\alpha_\eta}=\mathrm{diag}(5.4,6.2,5.0)$, and $K_o=0.1$.

Ground bench experiments of attitude tracking are conducted on a testbed. The incorporated onboard autopilot is equipped with an 80 MHz ARM processor and a six-axis inertial measurement unit, ensuring precise data acquisition and rapid response. Given the discrepancies between the mathematical models and the actual CTR-eVTOL system on the testbed, the CTR-eVTOL's initial task is to stabilize its attitude. Subsequently, an attitude tracking experiment is first conducted for the roll angle ϕ: the reference signal in the roll channel is set to $20°$, while the reference signals for the pitch and yaw channels are set to $0°$. At $14.48s$, a 100% LOE fault is injected into the rotor $2\#$ and the experimental results in the roll channel are shown in Figure 4(c). Then, the same maneuver in the roll channel is executed by using AC and ASMC controllers, respectively. Similarly, experiments in the pitch and yaw channels are conducted, as shown in Figures 5 and 6. A 100% LOE fault is injected into the CTR-eVTOL during these experiments.

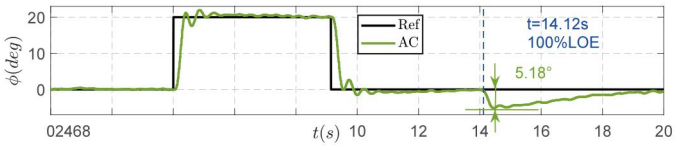

(a) Adaptive controller.

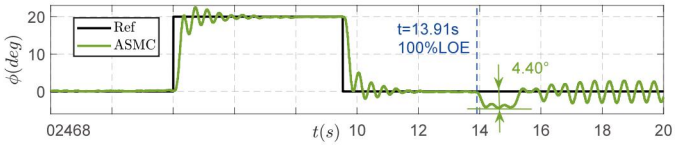

(b) ASMC controller.

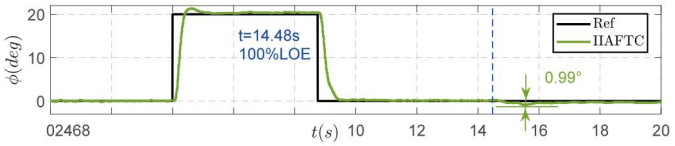

(c) IIAFTC strategy.

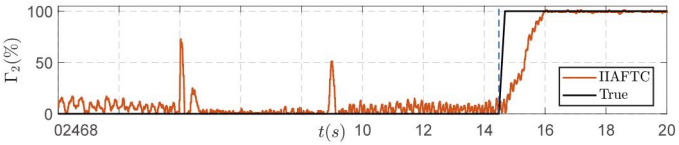

(d) Faulty coefficient estimation of the IIAFTC strategy.

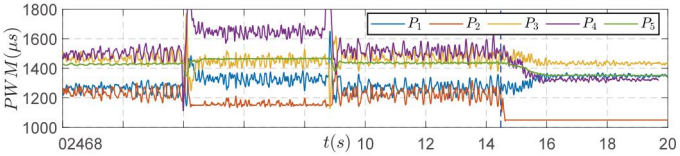

(e) PWM signals of the IIAFTC strategy.

Figure 4. Experimental results of attitude tracking for ϕ.

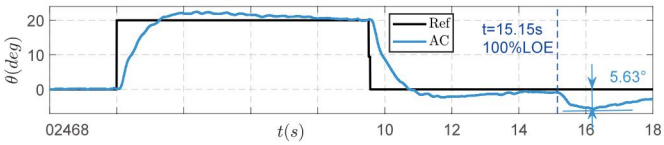

(a) Adaptive controller.

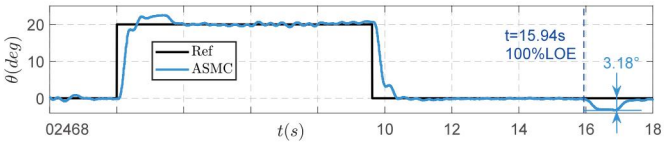

(b) ASMC controller.

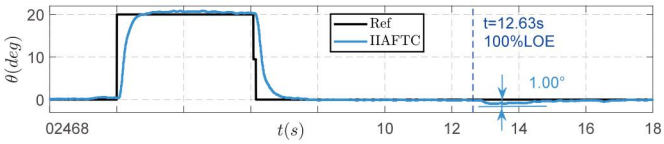

(c) IIAFTC strategy.

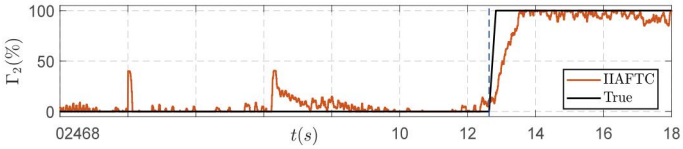

(d) Faulty coefficient estimation of the IIAFTC strategy.

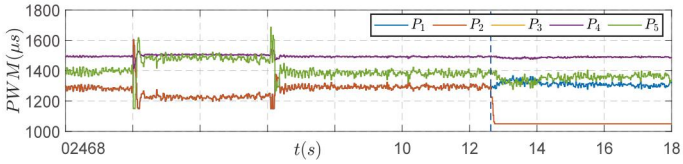

(e) PWM signals of the IIAFTC strategy.

Figure 5. Experimental results of attitude tracking for θ.

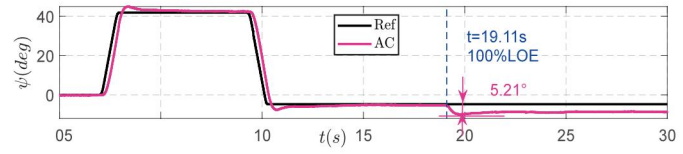

(a) Adaptive controller.

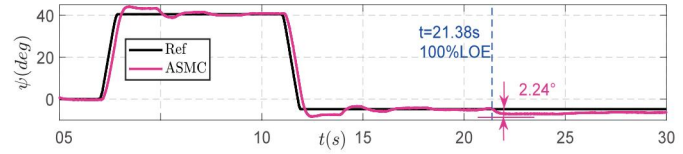

(b) ASMC controller.

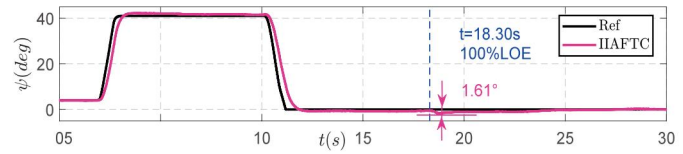

(c) IIAFTC strategy.

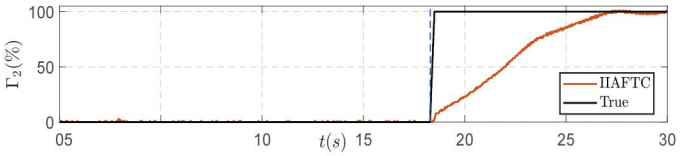

(d) Faulty coefficient estimation of the IIAFTC strategy.

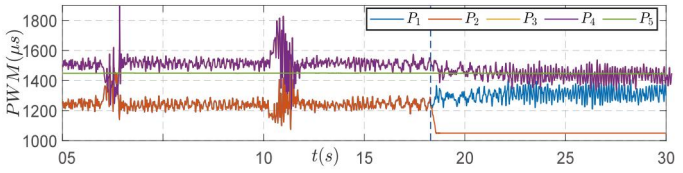

(e) PWM signals of the IIAFTC strategy.

Figure 6. Experimental results of attitude tracking for ψ.

Table 1. Comparison results of experiments.

	Max offset
IIAFTC	0.99° (↓77.5%), 1.00° (↓68.2%), 1.61° (↓28.1%)
AC	5.18°,5.63°, 5.21°
ASMC	4.40°, 3.14°, 2.24°
	RMSE
IIAFTC	1.28° (↓3.0%),1.17° (↓17.0%), 1.11° (↓12.6%)
AC	1.43°, 1.89°, 1.64°
ASMC	1.32°, 1.41°, 1.27°

Critical performance indices, including settling time, RMSE, and the max offset induced by an LOE fault, are summarized in Table 1. The designed IIAFTC strategy exhibits enhanced transient performance and stability in the presence of an LOE fault. For instance, in the direction ϕ, the maximum offset of the proposed strategy is $0.99°$, which is 77.5% less than that of the ASMC, and the RMSE decreases by 17.0% in direction θ. Furthermore, the estimated faulty coefficient $\hat{\Gamma}_2$ can converge to its true value Γ_2 as illustrated in Figure 4(d), which is consistent with the theoretical results in Theorem 1.

The above quantitative comparison demonstrates that the CTR-eVTOL equipped with the proposed IIAFTC strategy presents superior attitude tracking performance compared to other methods.

To further verify the effectiveness of the proposed strategy under partial LOE faults, ground bench experiments are conducted with gradually increasing partial LOE faults (30%, 60%, 100%). The attitude tracking and faulty coefficient estimation results are shown in Figs. 7–9, where the yellow area indicates a 30% LOE fault injected into rotor $2\#$, the pink area indicates a 60% LOE fault, and the red area indicates a 100% LOE fault. The experimental results demonstrate that the proposed IIAFTC strategy realize the estimation of the faulty coefficient and achieve attitude stabilization under multi-stage LOE faults.

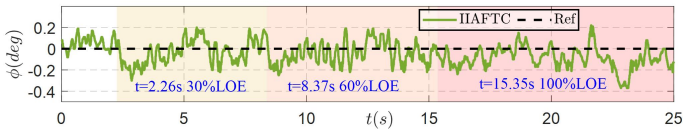

(a) IIAFTC strategy.

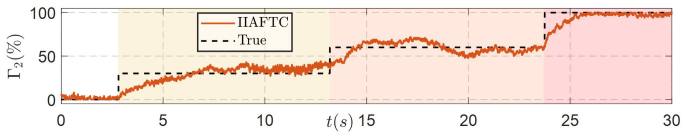

(b) Faulty coefficient estimation of the IIAFTC strategy.

Figure 7. Experimental results under partial LOE fault for ϕ.

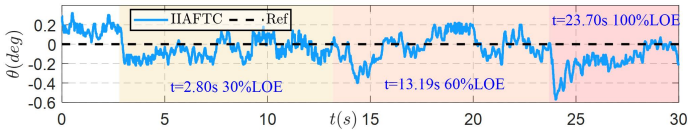

(a) IIAFTC strategy.

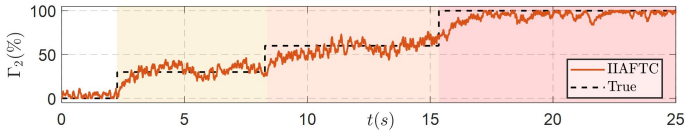

(b) Faulty coefficient estimation of the IIAFTC strategy.

Figure 8. Experimental results under partial LOE fault for θ.

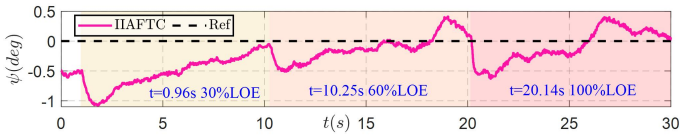

(a) IIAFTC strategy.

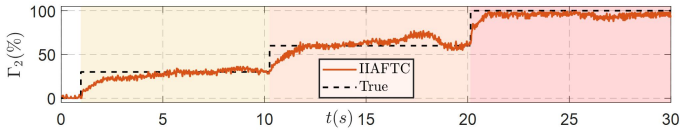

(b) Faulty coefficient estimation of the IIAFTC strategy.

Figure 9. Experimental results under partial LOE fault for ψ.

5. Conclusions

Under an LOE fault in one rotor, a nonlinear rigid-body dynamic model of the CTR-eVTOL is developed, explicitly accounting for the coupling effects between the upper and lower rotors within each CTR module. Based on the unique configuration of the CTR-eVTOL, an IIAFTC strategy is designed to compensate for the impact of LOE faults. This strategy ensures the convergence of the estimation error for the faulty coefficient and enables accurate attitude tracking with RMSE < 1.3°. The strategy outperforms traditional adaptive controllers with a 10.5% reduced RMSE and adaptive sliding mode controllers with a 3.0% reduced RMSE in the roll channel. In addition, ground bench experiments with gradually increasing partial LOE faults are also conducted. Currently, the strategy targets single-rotor LOE faults. Future work will focus on handling simultaneous faults and conducting outdoor flight validation.

Author Contributions: Conceptualization, Y.W. and Z.L.; methodology, Z.L. and Z.H.; validation, Z.H.; formal analysis, Y.W; investigation, Y.W. and Z.L.; writing—original draft preparation, Z.H.; writing—review and editing, Y.W. and Z.L.; visualization, Z.H. and Z.L.; supervision, Y.W.; funding acquisition, Y.W. All the authors have read and agreed to the published version of the manuscript.

Funding: This work was supported by the National Natural Science Foundation of China under Grants U24A20263 and 62203086.

Ethical Approval: Not applicable.

Informed Consent Statement: Not applicable.

Data Availability Statement: Not applicable.

Acknowledgments: None.

Conflicts of Interest: The authors declare no conflicts of interest.

References

[1] Milz, D.; May, M.S.; Looye, G. Dynamic Inversion-Based Control Concept for Transformational Tilt-Wing eVTOLs. In *Proceedings of the AIAA SciTech 2024 Forum*; 2024; p. 1290.

[2] Huang, H.; Su, J.; Wang, F.-Y. The Potential of Low-Altitude Airspace: The Future of Urban Air Transportation. *IEEE Trans. Intell. Veh.* **2024**, *9*, 5250–5254.

[3] Su, J.; Huang, H.; Zhang, H.; Wang, Y.; Wang, F.-Y. eVTOL Performance Analysis: A Review From Control Perspectives. *IEEE Trans. Intell. Veh.* **2024**, *9*, 4877–4889.

[4] Yokota, K.; Fujimoto, H. Aerodynamic force control for tilt-wing eVTOL using airflow vector estimation. *IEEE Trans. Transp. Electrif.* **2022**, *8*, 4163–4172.

[5] Li, D.; Zhang, L.; Mo, C.; Cui, N. Application of improved appointed time control in helicopter mode of a tilt-rotor eVTOL aircraft. *Aerosp. Sci. Technol.* **2024**, *153*, 109447.

[6] Lv, Z.-Y.; Wu, Y.; Zhao, Q.; Sun, X.-M. Design and control of a novel coaxial tilt-rotor UAV. *IEEE Trans. Ind. Electron.* **2022**, *69*, 3810–3821.

[7] Lv, Z.; Zhao, Q.; Sun, X.-M.; Wu, Y. Finite-time control design for a coaxial tilt-rotor UAV. *IEEE Trans. Ind. Electron.* **2024**, *71*, 16132–16142.

[8] Hou, Z.; Chen, L.; Lv, Z.; Wu, Y.; Song, H.; Wang, M. Nonsingular fast terminal sliding mode attitude control design for a coaxial tilt-rotor UAV. In *Proceedings of the 2024 SICE Festival with Annual Conference (SICE FES)*; IEEE: 2024; pp. 678–683.

[9] Zou, Y.; Xia, K. Robust fault-tolerant control for

underactuated takeoff and landing UAVs. *IEEE Trans. Aerosp. Electron. Syst.* **2020**, *56*, 3545–3555.

[10] Hao, W.; Xian, B.; Xie, T. Fault-tolerant position tracking control design for a tilt tri-rotor unmanned aerial vehicle. *IEEE Trans. Ind. Electron.* **2021**, *69*, 604–612.

[11] Guo, K.; Zhang, W.; Zhu, Y.; Jia, J.; Yu, X.; Zhang, Y. Safety control for quadrotor UAV against ground effect and blade damage. *IEEE Trans. Ind. Electron.* **2022**, *69*, 13373–13383.

[12] Nan, F.; Sun, S.; Foehn, P.; Scaramuzza, D. Nonlinear MPC for quadrotor fault-tolerant control. *IEEE Robot. Autom. Lett.* **2022**, *7*, 5047–5054.

[13] Chen, F.; Jiang, R.; Zhang, K.; Jiang, B.; Tao, G. Robust backstepping sliding-mode control and observer-based fault estimation for a quadrotor UAV. *IEEE Trans. Ind. Electron.* **2016**, *63*, 5044–5056.

[14] Wang, B.; Zhang, Y. An adaptive fault-tolerant sliding mode control allocation scheme for multirotor helicopter subject to simultaneous actuator faults. *IEEE Trans. Ind. Electron.* **2017**, *65*, 4227–4236.

[15] Slotine, J.-J.E.; Li, W. *Applied Nonlinear Control*; 1991; Vol. 199, No. 1.

[16] Astolfi, A.; Ortega, R. Immersion and invariance: a new tool for stabilization and adaptive control of nonlinear systems. *IEEE Trans. Autom. Control* **2003**, *48*, 590–606.

[17] Hu, J.; Zhang, H. Immersion and invariance based command filtered adaptive backstepping control of VTOL vehicles. *Automatica* **2013**, *49*, 2160–2167.

[18] Zhao, B.; Xian, B.; Zhang, Y.; Zhang, X. Nonlinear robust adaptive tracking control of a quadrotor UAV via immersion and invariance methodology. *IEEE Trans. Ind. Electron.* **2015**, *62*, 2891–2902.

[19] Chen, L.; Lv, Z.; Shen, X.; Wu, Y.; Sun, X.-M. Adaptive attitude control for a coaxial tilt-rotor UAV via immersion and invariance methodology. *IEEE/CAA J. Autom. Sin.* **2022**, *9*, 1710–1713.

[20] Zou, Y.; Xia, K. Robust fault-tolerant control for underactuated takeoff and landing UAVs. *IEEE Trans. Aerosp. Electron. Syst.* **2020**, *56*, 3545–3555.

[21] Chen, M.; Yan, K.; Wu, Q. Multi approximator-based fault tolerant tracking control for unmanned autonomous helicopter with input saturation. *IEEE Trans. Syst. Man Cybern. Syst.* **2021**, *52*, 5710–5722.

[22] Zhang, Z.; Xie, S.; Chen, Q. Disturbance observer-based singularity-free predefined-time attitude tracking control of quadrotors: theory and experiments. *IEEE Trans. Aerosp. Electron. Syst.* **2024**, *61*, 314–324.

[23] Tao, M.; Chen, Q.; He, X.; Xie, S. Fixed-time filtered adaptive parameter estimation and attitude control for quadrotor UAVs. *IEEE Trans. Aerosp. Electron. Syst.* **2024**, *58*, 4135–4146.

[24] Bobal, V. Technical note self-tuning Ziegler-Nichols PID controller. *Int. J. Adapt. Control Signal Process.* **1995**, *9*, 213–226.